Convolutional perfectly matched layer for elastic second-order wave equation

YiFeng Li, Olivier Bou Matar, and DF

Citation: The Journal of the Acoustical Society of America **127**, 1318 (2010); doi: 10.1121/1.3290999
View online: http://dx.doi.org/10.1121/1.3290999
View Table of Contents: http://asa.scitation.org/toc/jas/127/3
Published by the Acoustical Society of America

Convolutional perfectly matched layer for elastic second-order wave equation

YiFeng Li and Olivier Bou Matar[a)]
Joint European Laboratory LEMAC, Institut d'Electronique, de Microelectronique et de Nanotechnologie (IEMN-DOAE-UMR CNRS 8520), Ecole Centrale de Lille, 59651 Villeneuve d'Ascq, France

(Received 14 April 2009; revised 25 September 2009; accepted 17 December 2009)

In this work, a method is presented to extend the convolutional perfectly matched layer (C-PML) to simulate acoustic wave propagation in elastic media with a second-order equation formulation. This non-physical layer is used at the computational edge of a finite element method algorithm in frequency domain, and a pseudo-spectral algorithm in time domain, as an absorbing boundary condition (ABC) to truncate unbounded media. Numerical results show that the C-PML ABC attenuates the outgoing surface waves more effectively than classical PML ABC as proposed by Berenger [J. Comput. Phys. **114**, 195–200 (1994)] for electromagnetic waves in the case of oblique incidence, where the PML method suffers from large spurious reflections. Moreover, a modification of the proposed C-PML formulation is also discussed in order to stabilize the absorbing layer in anisotropic solids where numerical instabilities can appear.
 [DOI: 10.1121/1.3290999]

PACS number(s): 43.40.Fz, 43.20.Bi, 43.20.Fn, 43.20.Gp [DF] Pages: 1318–1327

I. INTRODUCTION

Numerical solutions of partial differential equations for wave propagation require the truncation of an unbounded media to fit into computers with a limited memory and computation time. For such problems, absorbing boundary conditions (ABCs) are needed at the truncated boundary to eliminate the reflections from this boundary to the computational domain.

In 1994, a new ABC, called perfectly matched layer (PML), has been introduced by Berenger[1] for electromagnetic waves. It has been proven to be the most robust and efficient technique for the termination of unbounded domain.[2] Since then, the technique has become classical in numerical simulation of wave propagation and has been extended, among others, for acoustic[3] and elastic waves in isotropic[4,5] and anisotropic media.[6] It has been proven that theoretically at the interface between a physical medium and a perfectly matched medium no reflection occurs, and the incident waves from the physical medium are completely absorbed, regardless of their incidence angle and frequency.[1,4] Nevertheless, this property will be lost when a discretization is needed for numerical implementation, especially in the case of oblique incidence. One then needs to optimize the PML parameters in order to decrease parasitic reflections.[7]

Convolutional perfectly matched layer (C-PML), first presented in electromagnetism by Roden and Gedney[8] and applied in the simulation of elastic wave propagation,[9–12] has been shown to improve the behavior of the discrete PML for grazing angle encountered in the case of surface waves. The main advantage of C-PML over the classical PML is that it is based on the unsplit components of the wave field and leads to a more stable scheme. Moreover, it is highly effective at absorbing signals of long time-signature,[13] surface waves,[12] or in elongated domains of calculation.[10]

Classically, C-PML has been introduced in first-order formulation of both electromagnetism and elastodynamics. In this paper, we propose to extend the C-PML absorbing layer to the second-order system describing elastic waves in displacement formulation in anisotropic solids, as it was done for classical split PML.[14] This second-order formulation will be described in frequency and time domains. In frequency domain, this technique is easy to implement in commercial software based on finite element method (FEM).

The efficiency of this second-order perfectly matched layer is demonstrated based on two dimensional (2D) benchmarks both for isotropic and anisotropic solids and for bulk and surface wave propagation. The simulations are realized with the commercially available software COMSOL MULTIPHYSICS in frequency domain and with a pseudo-spectral (PS) method in time domain. In some anisotropic media, numerical instabilities appear in the C-PML, and a modification of the proposed formulation is also discussed in order to stabilize the absorbing layer.

II. SECOND-ORDER FORMULATION OF ELASTIC WAVE PROPAGATION

Consider the propagation of 2D plane strain elastic waves in an anisotropic elastic solid medium. With Einstein's convention of summation, the equation of motion can be written as

$$\frac{\partial^2 u_i}{\partial t^2} = \frac{1}{\rho_0}\frac{\partial \tau_{ij}}{\partial x_j}, \tag{1}$$

where $i,j=1,2$, ρ_0 is the density, x_j are the components of the position vector, t is the time, u_i are the components of the particle displacement vector, and τ_{ij} are the components of

a)Author to whom correspondence should be addressed. Electronic mail: olivier.boumatar@iemn.univ-lille1.fr

the stress tensor. For a linear elastic solid, the constitutive relation is given by Hooke's law:

$$\tau_{ij} = C_{ijkl}\varepsilon_{kl}, \tag{2}$$

where C_{ijkl} are the elastic constants, and the linear approximation of the strain tensor $\boldsymbol{\varepsilon}$ is

$$\varepsilon_{kl} = \frac{1}{2}\left(\frac{\partial u_k}{\partial x_l} + \frac{\partial u_l}{\partial x_k}\right). \tag{3}$$

In the case of a transverse isotopic medium, the following second-order system of equation is obtained:

$$\frac{\partial^2 u_1}{\partial t^2} = \frac{1}{\rho_0}\left(\frac{\partial \tau_{11}}{\partial x} + \frac{\partial \tau_{12}}{\partial y}\right), \tag{4a}$$

$$\frac{\partial^2 u_2}{\partial t^2} = \frac{1}{\rho_0}\left(\frac{\partial \tau_{12}}{\partial x} + \frac{\partial \tau_{22}}{\partial y}\right), \tag{4b}$$

$$\tau_{11} = C_{11}\frac{\partial u_1}{\partial x} + C_{12}\frac{\partial u_2}{\partial y}, \tag{4c}$$

$$\tau_{22} = C_{12}\frac{\partial u_1}{\partial x} + C_{22}\frac{\partial u_2}{\partial y}, \tag{4d}$$

$$\tau_{12} = C_{66}\left(\frac{\partial u_1}{\partial y} + \frac{\partial u_2}{\partial x}\right). \tag{4e}$$

Here we have considered that $x_1 = x$ and $x_2 = y$. This system will be used as the starting point in the remainder of the paper.

III. C-PML FOR ELASTIC WAVE EQUATIONS IN FREQUENCY DOMAIN

Here, the methodology used for the introduction of C-PML zones for axisymmetric active solid media[9] is used for the system of Eq. (4). First, taking Fourier transform of the system, it is rewritten in the frequency domain. Then, the following complex coordinate transformation[15] is used:

$$\tilde{x} = \int_0^x s_x(x')dx', \tag{5a}$$

$$\tilde{y} = \int_0^y s_y(y')dy', \tag{5b}$$

where s_x and s_y are the complex frequency shifted (CFS) stretched-coordinate metrics proposed by Kuzuoglu and Mittra:[16]

$$s_x(x) = \kappa_x(x) + \frac{\sigma_x(x)}{\alpha_x(x) + j\omega}, \tag{6a}$$

$$s_y(y) = \kappa_y(y) + \frac{\sigma_y(y)}{\alpha_y(y) + j\omega}. \tag{6b}$$

α_x, σ_x, α_y, and σ_y are assumed to be positive and real, and κ_x and κ_y are real and ≥ 1. The $\sigma_{x,y}$ and $\kappa_{x,y}$ are the so-called[2] attenuation factor used for the attenuation of propagating waves and scaling factor used for the attenuation of evanescent waves, respectively. The $\alpha_{x,y}$ are frequency-dependent terms that implement a Butterworth-type filter in the layer. The originally split PML, introduced for isotropic elastic wave propagation by Chew and Liu[4] and for anisotropic solid by Collino and Tsogka,[6] is retrieved imposing $\alpha_{x,y} = 0$ and $\kappa_{x,y} = 1$. Using the complex coordinate variables $\tilde{x}$ and $\tilde{y}$ to replace x and y in Eqs. (4a)–(4e) and noting that $\partial/\partial\tilde{x} = (1/s_x)\,\partial/\partial x$ and $\partial/\partial\tilde{y} = (1/s_y)\,\partial/\partial y$, we obtain the following frequency domain equations in Cartesian coordinates:

$$-\omega^2\rho_0\hat{u}_1 = \frac{1}{s_x}\frac{\partial \hat{\tau}_{11}}{\partial x} + \frac{1}{s_y}\frac{\partial \hat{\tau}_{12}}{\partial y}, \tag{7a}$$

$$-\omega^2\rho_0\hat{u}_2 = \frac{1}{s_x}\frac{\partial \hat{\tau}_{12}}{\partial x} + \frac{1}{s_y}\frac{\partial \hat{\tau}_{22}}{\partial y}, \tag{7b}$$

$$\hat{\tau}_{11} = C_{11}\frac{1}{s_x}\frac{\partial \hat{u}_1}{\partial x} + C_{12}\frac{1}{s_y}\frac{\partial \hat{u}_2}{\partial y}, \tag{7c}$$

$$\hat{\tau}_{22} = C_{12}\frac{1}{s_x}\frac{\partial \hat{u}_1}{\partial x} + C_{22}\frac{1}{s_y}\frac{\partial \hat{u}_2}{\partial y}, \tag{7d}$$

$$\hat{\tau}_{12} = C_{66}\left(\frac{1}{s_y}\frac{\partial \hat{u}_1}{\partial y} + \frac{1}{s_x}\frac{\partial \hat{u}_2}{\partial x}\right), \tag{7e}$$

where $\hat{u}$ represents the Fourier transform of the variable u.

In order to implement this C-PML in a commercial FEM software (COMSOL MULTIPHYSICS), the resulting second-order C-PML wave equations are interpreted as an anisotropic medium, as it has already been done for PML.[17] Multiplying Eq. (7) by $s_x s_y$ and introducing new stress tensor $\hat{\tau}'_{ij}$ and density ρ'_0 (given by $\rho_0 s_x s_y$), we get the following equations:

$$-\omega^2\rho'_0\hat{u}_1 = \frac{\partial \hat{\tau}'_{11}}{\partial x} + \frac{\partial \hat{\tau}'_{12}}{\partial y}, \tag{8a}$$

$$-\omega^2\rho'_0\hat{u}_2 = \frac{\partial \hat{\tau}'_{21}}{\partial x} + \frac{\partial \hat{\tau}'_{22}}{\partial y}, \tag{8b}$$

$$\hat{\tau}'_{11} = \hat{\tau}_{11}s_y = C_{11}\frac{s_y}{s_x}\frac{\partial \hat{u}_1}{\partial x} + C_{12}\frac{\partial \hat{u}_2}{\partial y}, \tag{8c}$$

$$\hat{\tau}'_{22} = \hat{\tau}_{22}s_x = C_{12}\frac{\partial \hat{u}_1}{\partial x} + C_{22}\frac{s_x}{s_y}\frac{\partial \hat{u}_2}{\partial y}, \tag{8d}$$

$$\hat{\tau}'_{12} = \hat{\tau}_{12}s_x = C_{66}\left(\frac{s_x}{s_y}\frac{\partial \hat{u}_1}{\partial y} + \frac{\partial \hat{u}_2}{\partial x}\right), \tag{8e}$$

$$\hat{\tau}'_{21} = \hat{\tau}_{12}s_y = C_{66}\left(\frac{\partial \hat{u}_1}{\partial y} + \frac{s_y}{s_x}\frac{\partial \hat{u}_2}{\partial x}\right). \tag{8f}$$

This system of equation corresponds to the propagation of elastic waves in a "fictious" anisotropic medium and can be written in the matrix form as

$$\begin{bmatrix} \hat{\tau}'_{11} \\ \hat{\tau}'_{22} \\ \hat{\tau}'_{12} \\ \hat{\tau}'_{21} \end{bmatrix} = \begin{bmatrix} C'_{11} & C_{12} & 0 & 0 \\ C_{12} & C'_{22} & 0 & 0 \\ 0 & 0 & C'_{66} & C_{66} \\ 0 & 0 & C_{66} & C''_{66} \end{bmatrix} \begin{bmatrix} u_{1,x} \\ u_{2,y} \\ u_{1,y} \\ u_{2,x} \end{bmatrix}, \tag{9}$$

with $u_{1,x}=\partial\hat{u}_1/\partial x$, $u_{2,y}=\partial\hat{u}_2/\partial y$, $u_{1,y}=\partial\hat{u}_1/\partial y$, and $u_{2,x}=\partial\hat{u}_2/\partial x$. The new effective elastic stiffnesses are $C'_{11}=C_{11}s_y/s_x$, $C'_{22}=C_{22}s_x/s_y$, $C'_{66}=C_{66}s_x/s_y$, and $C''_{66}=C_{66}s_y/s_x$. It should be noted that this fictious anisotropic medium has a nonsymmetric stress tensor ($\hat{\tau}_{ij}\neq\hat{\tau}_{ji}$ when $i\neq j$), and the complex-valued tensor of elastic constants conserves minor symmetry properties, but not the major one.

We can easily extend this description of C-PML in anisotropic solid to three dimensions. In this case, the general form of the propagation of elastic waves can be described as

$$-\omega^2\rho'_0\hat{u}_i=\frac{\partial\hat{\tau}'_{ij}}{\partial x_j}, \tag{10a}$$

$$\hat{\tau}'_{ij}=C'_{ijkl}\frac{\partial\hat{u}_l}{\partial x_k}, \tag{10b}$$

where $i,j,k,l=1$, 2, or 3. The effective elastic tensor C' and the density ρ'_0 are given by

$$C'_{ijkl}=C_{ijkl}\frac{s_xs_ys_z}{s_is_k}, \tag{11a}$$

$$\rho'_0=\rho_0s_xs_ys_z. \tag{11b}$$

The effective constants already obtained for 2D situation can be easily derived from Eq. (11a) by considering that $s_z=1$ and $i,j,k,l=1$ or 2. Moreover, this fictious anisotropic interpretation of C-PML or PML can be extended to piezoelectric solids.[18–20]

IV. C-PML FOR ELASTIC WAVE EQUATIONS IN TIME DOMAIN

Now, to be able to obtain a C-PML formulation in time domain, the resulting equations are transformed back to time domain by inverse Fourier transform. Due to the frequency dependence of the CFS stretched-coordinate metrics, a convolution appears in the resulting equations, as shown, for example, for Eq. (7a):

$$\frac{\partial^2u_1}{\partial t^2}=\frac{1}{\rho_0}\left[F^{-1}\left[\frac{1}{s_x}\right]\otimes\frac{\partial\tau_{11}}{\partial x}+F^{-1}\left[\frac{1}{s_y}\right]\otimes\frac{\partial\tau_{12}}{\partial y}\right], \tag{12}$$

where $\otimes$ and $F^{-1}[\cdot]$ are, respectively, the convolution and inverse Fourier transform operators. In order to eliminate the convolutions appearing in Eq. (12), we use the methodology introduced by Roden and Gedney[8] in electromagnetism and extended by Bou Matar *et al.*[9] for elastic wave propagation in active (or nonlinear) media by introducing memory variables. The time evolution of each of these memory variables is realized by a first-order differential equation. The obtained result can be rewritten as

$$\frac{\partial^2u_1}{\partial t^2}=\frac{1}{\rho_0}\left(\frac{1}{\kappa_x}\frac{\partial\tau_{11}}{\partial x}+\frac{1}{\kappa_y}\frac{\partial\tau_{12}}{\partial y}+\frac{A_x}{\kappa_x}+\frac{B_y}{\kappa_y}\right), \tag{13}$$

where the memory variables A_x and B_y are given by

$$\frac{\partial A_x}{\partial t}=-\delta_x\frac{\partial\tau_{11}}{\partial x}-\beta_xA_x, \tag{14a}$$

$$\frac{\partial B_y}{\partial t}=-\delta_y\frac{\partial\tau_{12}}{\partial y}-\beta_yB_y, \tag{14b}$$

with $\delta_{x,y}=\sigma_{x,y}/\kappa_{x,y}$ and $\beta_{x,y}=\sigma_{x,y}/\kappa_{x,y}+\alpha_{x,y}$. Making the same calculation for Eqs. (7b)–(7e), we obtain the following system equations of C-PML in time domain for elastic wave propagation in anisotropic solid:

$$\frac{\partial^2u_1}{\partial t^2}=\frac{1}{\rho_0}\left(\frac{1}{\kappa_x}\frac{\partial\tau_{11}}{\partial x}+\frac{1}{\kappa_y}\frac{\partial\tau_{12}}{\partial y}+\frac{A_x}{\kappa_x}+\frac{B_y}{\kappa_y}\right), \tag{15a}$$

$$\frac{\partial^2u_2}{\partial t^2}=\frac{1}{\rho_0}\left(\frac{1}{\kappa_x}\frac{\partial\tau_{12}}{\partial x}+\frac{1}{\kappa_y}\frac{\partial\tau_{22}}{\partial y}+\frac{C_x}{\kappa_x}+\frac{D_y}{\kappa_y}\right), \tag{15b}$$

$$\tau_{11}=\frac{C_{11}}{\kappa_x}\frac{\partial u_1}{\partial x}+\frac{C_{12}}{\kappa_y}\frac{\partial u_2}{\partial y}+\frac{C_{11}}{\kappa_x}E_x+\frac{C_{12}}{\kappa_y}F_y, \tag{15c}$$

$$\tau_{22}=\frac{C_{12}}{\kappa_x}\frac{\partial u_1}{\partial x}+\frac{C_{22}}{\kappa_y}\frac{\partial u_2}{\partial y}+\frac{C_{12}}{\kappa_x}E_x+\frac{C_{22}}{\kappa_y}F_y, \tag{15d}$$

$$\tau_{12}=\frac{C_{66}}{\kappa_x}\frac{\partial u_2}{\partial x}+\frac{C_{66}}{\kappa_y}\frac{\partial u_1}{\partial y}+\frac{C_{66}}{\kappa_x}G_x+\frac{C_{66}}{\kappa_y}H_y, \tag{15e}$$

where the memory variables C_x, D_y, E_x, F_y, G_x, and H_y are obtained by the first-order differential equations similar to the one derived for A_x and B_y in Eq. (14). The memory variables will be zero outside the C-PML zones, so the first-order differential equations of memory variables need only to be solved in a small part of the calculation domain. After introducing Eqs. (15c)–(15e) into Eqs. (15a) and (15b), the resulting system of wave equations can be written as

$$\rho_0\frac{\partial^2u_1}{\partial t^2}-\left[\frac{\partial}{\partial x}\left(C_{11}\frac{\partial u_1}{\partial x}+C_{12}\frac{\partial u_2}{\partial y}\right)+\frac{\partial}{\partial y}\left(C_{66}\frac{\partial u_2}{\partial x}+C_{66}\frac{\partial u_1}{\partial y}\right)\right]=f_1, \tag{16a}$$

$$\rho_0\frac{\partial^2u_2}{\partial t^2}-\frac{\partial}{\partial x}\left(C_{66}\frac{\partial u_2}{\partial x}+C_{66}\frac{\partial u_1}{\partial y}\right)+\frac{\partial}{\partial y}\left(C_{12}\frac{\partial u_1}{\partial x}+C_{22}\frac{\partial u_2}{\partial y}\right)=f_2, \tag{16b}$$

where f_1 and f_2 are

$$f_1 = \left[-\frac{\kappa'_x}{\kappa_x}\frac{\partial}{\partial x}\left(\frac{C_{11}}{\kappa_x}\frac{\partial u_1}{\partial x} + \frac{C_{12}}{\kappa_y}\frac{\partial u_2}{\partial y} + \frac{C_{11}}{\kappa_x}E_x + \frac{C_{12}}{\kappa_y}F_y\right) - \frac{\kappa'_y}{\kappa_y}\frac{\partial}{\partial y}\left(\frac{C_{66}}{\kappa_x}\frac{\partial u_2}{\partial x} + \frac{C_{66}}{\kappa_y}\frac{\partial u_1}{\partial y} + \frac{C_{66}}{\kappa_x}G_x + \frac{C_{66}}{\kappa_y}H_y\right) - \frac{\partial}{\partial x}\left(\frac{\kappa'_x C_{11}}{\kappa_x}\frac{\partial u_1}{\partial x} + \frac{\kappa'_y C_{12}}{\kappa_y}\frac{\partial u_2}{\partial y} - \frac{C_{11}}{\kappa_x}E_x - \frac{C_{12}}{\kappa_y}F_y\right) - \frac{\partial}{\partial y}\left(\frac{\kappa'_x C_{66}}{\kappa_x}\frac{\partial u_2}{\partial x} + \frac{\kappa'_y C_{66}}{\kappa_y}\frac{\partial u_1}{\partial y} - \frac{C_{66}}{\kappa_x}G_x - \frac{C_{66}}{\kappa_y}H_y\right) + \frac{A_x}{\kappa_x} + \frac{B_y}{\kappa_y}\right], \tag{16c}$$

$$f_2 = \left[-\frac{\kappa'_x}{\kappa_x}\frac{\partial}{\partial x}\left(\frac{C_{66}}{\kappa_x}\frac{\partial u_2}{\partial x} + \frac{C_{66}}{\kappa_y}\frac{\partial u_1}{\partial y} + \frac{C_{66}}{\kappa_x}G_x + \frac{C_{66}}{\kappa_y}H_y\right) - \frac{\kappa'_y}{\kappa_y}\frac{\partial}{\partial y}\left(\frac{C_{12}}{\kappa_x}\frac{\partial u_1}{\partial x} + \frac{C_{22}}{\kappa_y}\frac{\partial u_2}{\partial y} + \frac{C_{12}}{\kappa_x}E_x + \frac{C_{22}}{\kappa_y}F_y\right) - \frac{\partial}{\partial x}\left(\frac{\kappa'_x C_{66}}{\kappa_x}\frac{\partial u_2}{\partial x} + \frac{\kappa'_y C_{66}}{\kappa_y}\frac{\partial u_1}{\partial y} - \frac{C_{66}}{\kappa_x}G_x - \frac{C_{66}}{\kappa_y}H_y\right) - \frac{\partial}{\partial y}\left(\frac{\kappa'_x C_{12}}{\kappa_x}\frac{\partial u_1}{\partial x} + \frac{\kappa'_y C_{22}}{\kappa_y}\frac{\partial u_2}{\partial y} - \frac{C_{12}}{\kappa_x}E_x - \frac{C_{22}}{\kappa_y}F_y\right) + \frac{C_x}{\kappa_x} + \frac{D_y}{\kappa_y}\right], \tag{16d}$$

where we have introduced the notation $\kappa'_{x,y}=\kappa_{x,y}-1$. The formulation of C-PML given by Eq. (16) has been introduced in order to facilitate the implementation of the resulting second-order C-PML wave equations in commercial finite element packages and in our homemade PS code.

It is important to note that in time domain the number of equation needed to be solved increases in the C-PML zones. This can considerably increase the burden of calculation. Nevertheless, when active (or nonlinear) media are considered, then time domain formulations are needed,[9] and Eq. (16) has to be used. Moreover, the number of auxiliary variables in the unsplit and convolutional PML is less than the one of the classical split PML. In the considered case, elastic wave propagation in a 2D anisotropic solid, eight auxiliary variables are needed for the unsplit PML and ten for the split PML. In both cases, these auxiliary variables need to be stored in addition to the total field variables: u_1 and u_2 for the proposed CPML or u_1, u_2, τ_{11}, τ_{22}, and τ_{12} for the classical split PML. In the classical PML case, one can choose either to store or not the total field. In this last case, the memory storage is reduced but the computation time is increased because one then needs to compute the total field variables as the sum of two splitted auxiliary variables several times in each iteration of the time loop.

V. NUMERICAL TESTS

In this section, the excellent absorbing behaviors of both formulations (frequency and time domains) are demonstrated. The frequency domain formulation has been implemented in a commercial FEM software (COMSOL MULTIPHYSICS), and a PS code has been developed for the time domain formulation. The choice of these numerical schemes has been motivated by the compromise in obtaining both efficient and accurate methods for the two different formulations.

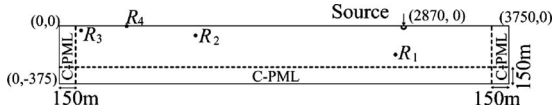

FIG. 1. Schematic of the model used in the example of surface wave in a homogeneous isotropic medium. The C-PML terminations are positioned at the left, right, and bottom sides of the simulation domain. The top boundary is a stress free boundary. The source and four receiver (R_1, R_2, R_3, and R_4) positions are also depicted.

A. Surface wave in a homogeneous isotropic medium

In order to demonstrate the improvement induced by the use of C-PML, instead of classical PML, numerical simulations of elastic wave propagation in a half space of homogeneous isotropic medium, similar to the ones proposed by Drossaert and Giannopoulos,[11] are presented. The sketch of the used elongated calculation domain (3750 m width and 375 m height, including the C-PMLs and corresponding to 200×20 grid elements) is given in Fig. 1, where the origin (0, 0) is at the left upper corner. The properties of the elastic medium have been chosen as follows: the density is $\rho_0=2000$ kg m^{-3}, and the Lame constants are $\lambda=0.6\times 10^9$ and $\mu=0.3\times 10^9$ N/m^2. A directional point source, acting as a force perpendicular to the upper free surface, is located at (2870.0, 0.0). Four receiving positions R_1, R_2, R_3, and R_4 are chosen at the following locations: (2800.0, −187.5), (1120.0, −42.5), (168.75, −18.75), and (562.5, 0), respectively. The choice of these receiving positions has been realized in order to demonstrate typical behavior of the C-PML. The temporal variation of the point source is a Ricker wavelet given by

$$f(t) = (0.5 + a_1(t-t_D)^2)e^{-a_1(t-t_D)^2}, \tag{17}$$

where $t_D=1.0$ s is the source delay time, $a_1=(\pi f_c)^2$, and $f_c=1.0$ Hz is the central frequency.

In the stretched-coordinate metrics, the following spatial coordinate dependences are used for the parameters of the C-PMLs in the x direction:

$$\kappa_x = 1 + \kappa_{\max}\left(\frac{x-x_0}{d_x}\right)^{n_1}, \tag{18a}$$

$$\sigma_x = \sigma_{\max}\left(\frac{x-x_0}{d_x}\right)^{n_1+n_2}, \tag{18b}$$

$$\alpha_x = \alpha_{\max}\left(\frac{d_x - x + x_0}{d_x}\right)^{n_3}, \tag{18c}$$

with $\alpha_{\max}=2\pi f_\alpha$ and

$$\sigma_{\max} = (1+n_1+n_2)\sqrt{(\lambda+2\mu)/\rho_0}\log(1/R_0)/(2d_x), \tag{19}$$

where R_0 is the reflection coefficient from the C-PML we want to obtain, and x_0 and d_x are, respectively, the starting position and thickness of the C-PML. κ_y, σ_y, and α_y have the

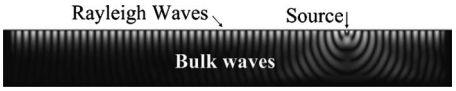

FIG. 2. Displacement amplitude snapshot at frequency 3 Hz for the model depicted in Fig. 1, showing the propagation and absorption in the C-PML terminations of both bulk and Rayleigh waves.

same form as κ_x, σ_x, and α_x, respectively, just replacing x by y. f_α is a characteristic frequency of the C-PML (here $f_\alpha = 10^{-2}$ Hz). It corresponds to a cut off frequency.[21] Indeed, when $f \gg f_\alpha$ the complex frequency shifted coefficients $\alpha_{x,y}$ are negligible, and the attenuation in the C-PML is the same as in the PML. On the other hand, when $f \ll f_\alpha$ the stretch of the coordinates is real and the medium does not absorb propagating waves, but only the evanescent waves. The spatial dependences used in Eq. (18) are the same as the ones classically proposed for PML applied to electromagnetic waves.[2] $\sigma_{\max}$ given by Eq. (19) corresponds to the optimal value proposed in Ref. 6. In the considered cases we use $\kappa_{\max}=0$. Moreover, $\kappa_{x,y}=1$ and $\sigma_{x,y}=0$ in the computational domain, outside the C-PML zone. In the presented results, a C-PML thickness of eight grid elements, both in the left, right, and bottom boundaries, $R_0=5\ \ 10^{-5}$, $n_1=3$, $n_2=0$, and $n_3=1$ has been chosen. We remind also that the classical PML case corresponds to $\alpha_{\max}=0$.

Here, Eq. (8) has been solved with COMSOL MULTIPHYSICS FEM software in frequency domain. Indeed, as demonstrated by Castaings *et al.*,[22] very efficient simulations of linear pulse propagation in solids can be obtained with only a limited number of frequency calculations. The time evolution of the point source [Eq. (17)] is first Fourier transform, and Eq. (8) is then solved for 40 frequencies equally spaced in the source spectrum. Second-order Lagrange elements have been used in all the FEM calculations. The result obtained at one frequency (3 Hz) is shown in Fig. 2, where both bulk waves in the physical domain and Rayleigh waves on the free surface boundary can be seen. In Fig. 3, the time evolutions of the horizontal [(a) and (b)] and vertical [(c) and (d)] displacements reconstructed by inverse Fourier transform of the 40 frequency responses at the fourth receiver, positioned at the free surface, in the case of both C-PML (dotted line) and PML (dashed line) layers for absorbing the surface wave are displayed and compared to an analytical solution (solid line). The FORTRAN code EX2DDIR of Berg *et al.*[23] has been used to compute this exact solution of the 2D response from a vertical directional point source in an isotropic elastic half space with a free surface. The obtained results clearly demonstrated the increased efficiency of the C-PML in comparison with the PML in order to absorb the Rayleigh wave, particularly when a zoom [Figs. 3(b) and 3(d)] is made around the end of this surface wave. This is in perfect accordance with previous results obtained with the C-PML first-order velocity-stress formulation implementation.[10–12]

The time evolutions of the horizontal [(a), (c), and (e)] and vertical [(b), (d), and (f)] displacements for the three other receivers (R_1, R_2, and R_3) in the case of FEM simulation with C-PML (dotted line) are plotted in Fig. 4 and compared, as before, with a FEM simulation with PML (dashed

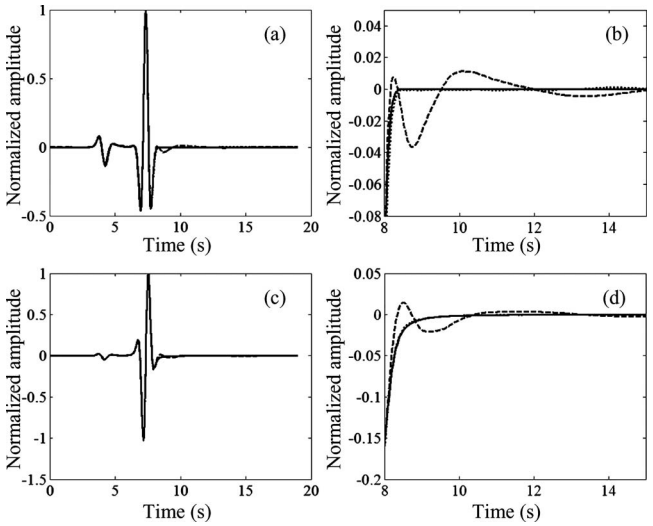

FIG. 3. Time evolution of the horizontal u_1 (a) and the vertical u_2 (c) components of the displacement vector at the fourth receiver of the analytical solution of the problem (solid line) and the numerical solution with PML (dashed line) and C-PML (dotted line). (b) and (d) are zoom of (a) and (c), respectively, showing the benefit of using C-PML instead of PML.

line) and an analytical solution (solid line). As in Fig. 3, it clearly appears in Fig. 4 that the use of C-PML greatly improves the surface wave absorption efficiency of the absorbing layer (see R_2 signal, where spurious oscillations of the horizontal displacement component are observed in the case

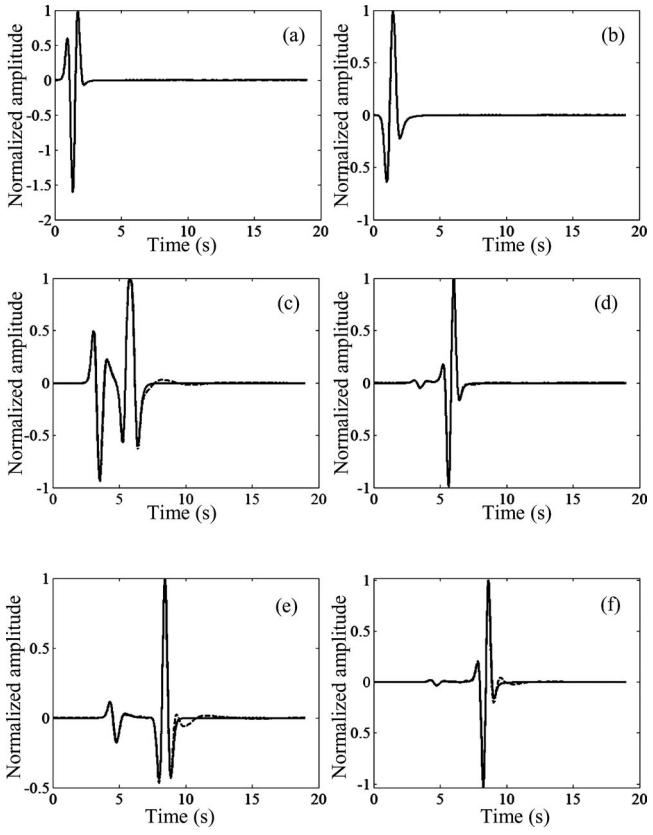

FIG. 4. Time evolution of the horizontal u_1 (left) and the vertical u_2 (right) components of the displacement vector at the first (top), second (middle), and third (bottom) receivers of the analytical solution of the problem (solid line) and the numerical solution with PML (dashed line) and C-PML (dotted line).

of PML), even if the receiver is positioned close to the absorbing layer, as for the R_3 receiver. It is linked to evanescent part of the Rayleigh wave in the bulk direction which interacts over a long distance with the PML at the bottom. In the case of the first receiver, placed in the bulk of the sample where the contribution of surface wave is negligible, the C-PML and PML have the same absorbing efficiency, and the overall agreement with the analytical solution is almost perfect.

B. Bulk wave in a homogeneous anisotropic medium

The PS code described in Ref. 9 has been modified in order to solve the second-order wave equation system of Eq. (16), in place of the classical first-order stress-particle velocity formulation used in finite difference time domain elastic wave propagation simulations. The forward integration in time, realized in our previous PS code by a staggered fourth-order Adams–Bashforth method, is here made with the use of a second-order finite difference method.

Simulations of pulse propagation in anisotropic solids have been made in order to demonstrate the efficiency of the proposed time domain C-PML formulation for second-order wave equations. The properties, density and elasticity coefficients, of the three different orthotropic materials used in the time domain simulations are shown in Table I. The choice of the material name (I, III, and V) has been made, following Bécache *et al.*,[24] in order to simplify the comparison of our results with previous ones.[24–26] In all cases, a 25 cm × 25 cm portion of an infinite solid has been discretized on a 128 × 128 element grid (including the ten element C-PML placed on each side), and a 5 ns time step was used. The following source term $f(x,y,t)$ is added to f_1 in the right hand side of Eq. (16a):

TABLE I. Properties of the orthotropic materials used in the time domain simulations.

Material	ρ (kg/m^3)	C_{11} (GPa)	C_{22} (GPa)	C_{12} (GPa)	C_{66} (GPa)
I	4000	40	200	38	20
III	4000	40	200	75	20
V	4000	300	60	99	15

$$f(x,y,t) = (0.5 + a_1(t - t_D)^2)e^{-a_1(t-t_D)^2}\frac{e^{-7[(x^2+y^2)/r_0^2]}}{r_0^2}, \quad (20)$$

where $a_1 = (\pi f_c)^2$, $f_c = 150$ kHz is the central frequency, $t_D = 1/f_c$ is the source delay time, and $r_0 = 5$ mm. It corresponds to a Gaussian spatial distribution around the (0,0) point which is placed at the center in all the simulations and to a Ricker wavelet time evolution. The same spatial coordinate dependences [Eq. (18)] are used for the C-PML parameters with now $\alpha_{\max} = 20\pi$, $n_1 = 2$, $n_2 = 1$, $n_3 = 1$, and

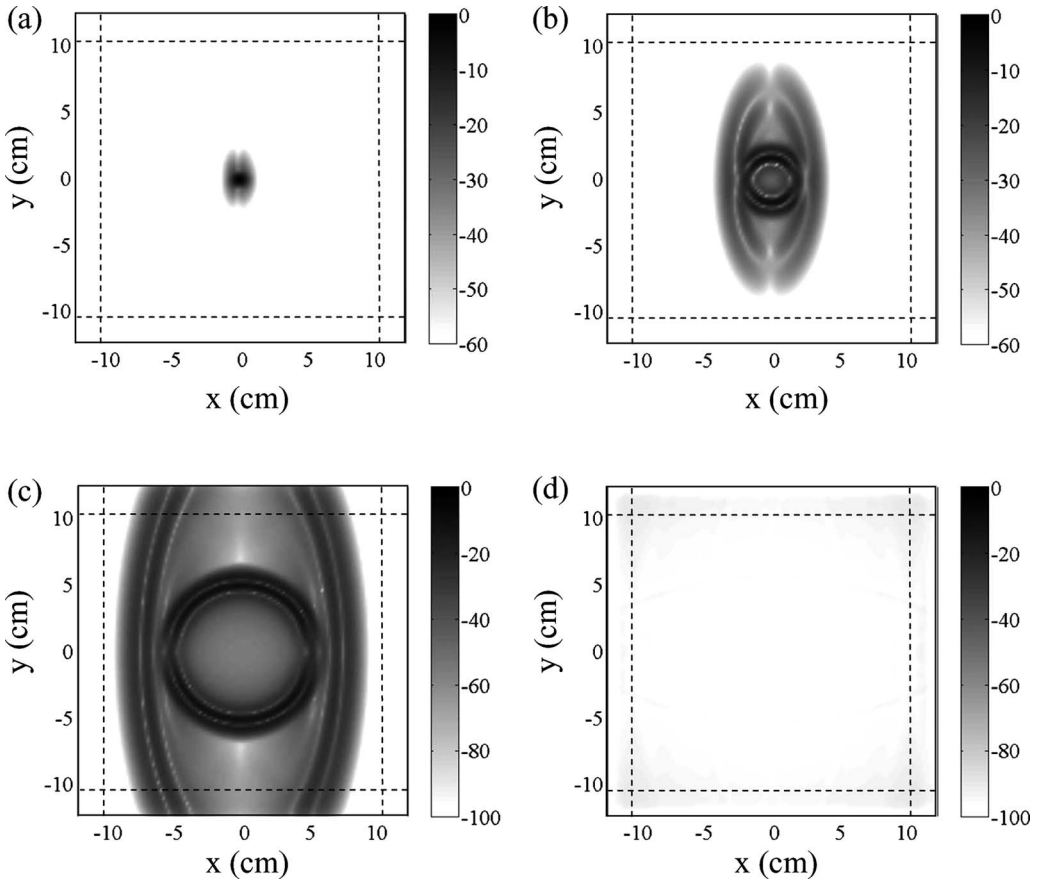

FIG. 5. Snapshots of propagation of the displacement magnitude in an orthotropic elastic medium, model I, at (a) $t = 5$ μs, (b) $t = 15$ μs, (c) $t = 30$ μs, and (d) $t = 125$ μs. The snapshots are in dB scale with a reference displacement amplitude of 10 nm.

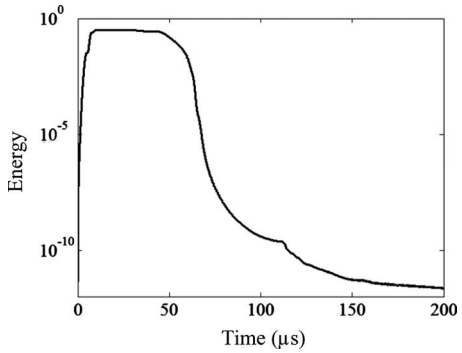

FIG. 6. Energy decay in the physical domain for the orthotropic elastic medium, model I, in the same conditions as the ones used to obtain the snapshots of Fig. 5.

$$\sigma_{\max} = (1 + n_1 + n_2)\sqrt{C_{11}/\rho_0}\log(1/R_0)/(2d_x), \tag{21}$$

where $R_0 = 10^{-12}$.

In Fig. 5, snapshots of the propagation of the amplitude of the displacement in medium I are displayed for four different times (5, 15, 30, and 125 μs). Here and in all the following figures, the snapshots presented are in dB scale with a reference displacement of 10 nm. The overall absorption of the C-PML is excellent and the level of spurious reflection is very small, only a −90 dB reflected pulse can be seen at the later time [Fig. 5(d)]. In order to see more quantitatively the quality of the C-PML, the total energy E at each time is computed according to the following expression:

$$E = \frac{1}{2}\int_\Omega \rho_0 \|\boldsymbol{v}\|^2 d\Omega + \frac{1}{2}\int_\Omega \tau_{ij}\varepsilon_{ij} d\Omega, \tag{22}$$

where Ω is the volume corresponding to the physical domain, and $\|\mathbf{v}\|$ is the magnitude of the velocity vector. Figure 6 displays the energy decay in the physical domain for the proposed C-PML model. The wave field has left the physical domain at about 60 μs here. This figure not only confirms that at later time the energy has decayed by a factor of 10^{12} but also demonstrates that no significant spurious reflection appears before.

Snapshots of the propagation of the amplitude of the displacement in medium III are displayed for four different times (5, 15, 30, and 50 μs) in Fig. 7. As all the other PML or C-PML implementations, some instabilities appear [Figs. 7(c) and 7(d)] in the absorbing layers where, as explained by Bécache *et al.*,[24] one of the incident elastic waves arrives with the components of the group velocity and the slowness vector, in the C-PML direction, of opposite signs. These instabilities are one of the major limitations in the use of PML for elastic waves propagating in anisotropic solids and in plates, even in the case of an isotropic medium.[27] In the case of elastic plate absorbing layers, solutions have been proposed in order to overcome this limitation, but at the expense

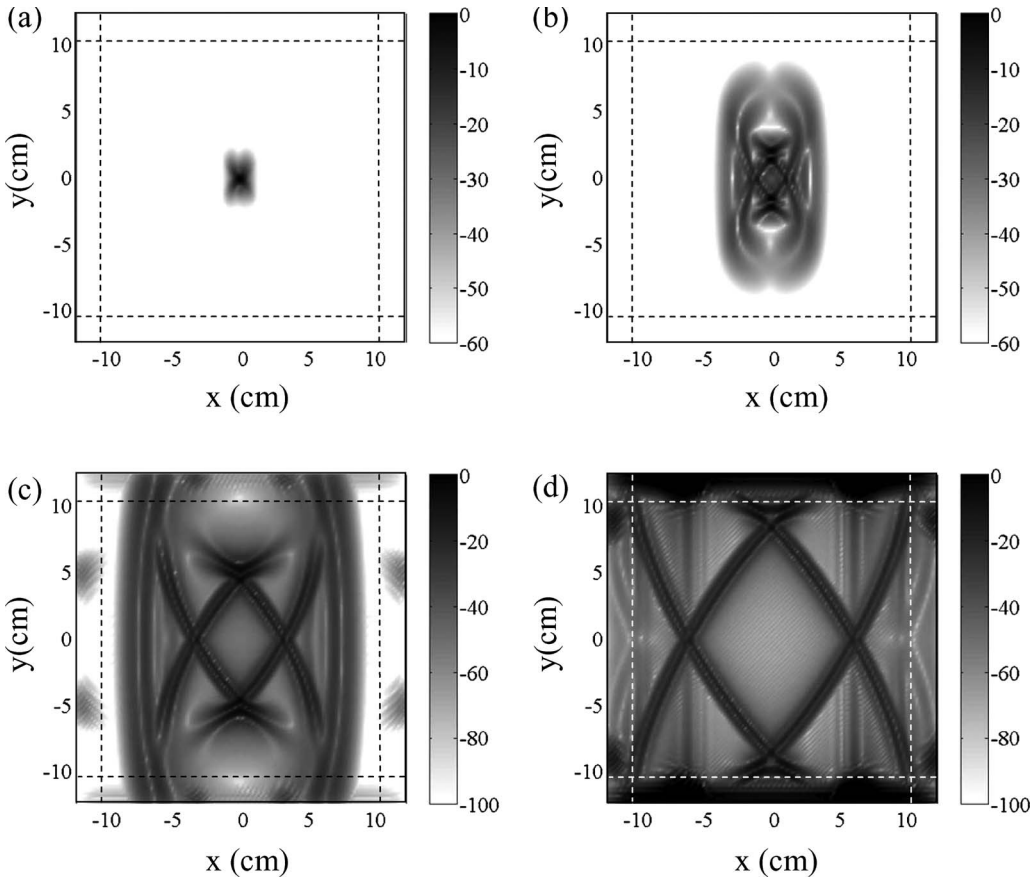

FIG. 7. Snapshots of propagation of the displacement magnitude in an orthotropic elastic medium, model III, at (a) $t=5$ μs, (b) $t=15$ μs, (c) $t=30$ μs, and (d) $t=50$ μs. The snapshots are in dB scale with a reference displacement amplitude of 10 nm. Instabilities are observed for the C-PML terminations used in the simulation.

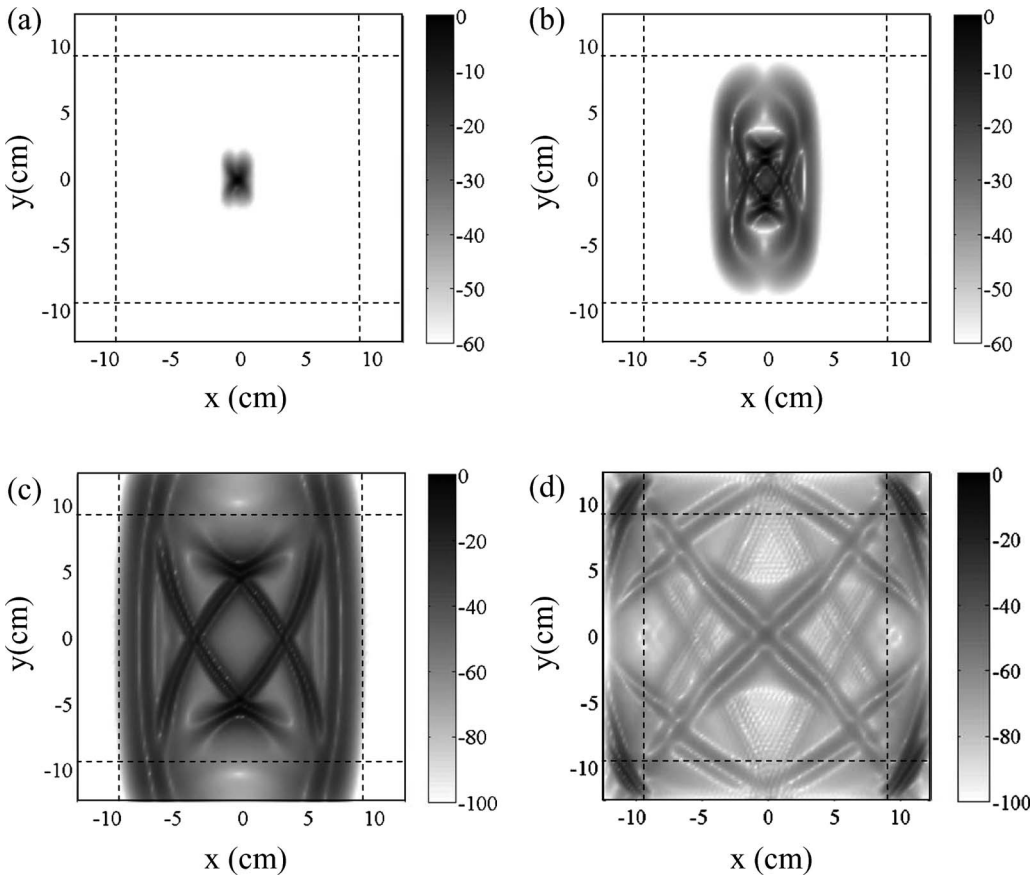

FIG. 8. Snapshots of propagation of the displacement magnitude in an orthotropic elastic medium, model III, at (a) $t=5$ μs, (b) $t=15$ μs, (c) $t=30$ μs, and (d) $t=125$ μs. The snapshots are in dB scale with a reference displacement amplitude of 10 nm. No instability is observed for the M-PML terminations used in the simulation.

of an increased length of the absorbing zone.[18,22,28] An elegant way of preserving the use of short length PML has been introduced by Skelton *et al.*,[29] but at the expense now of having one different PML for each propagating mode. For anisotropic solids an absorbing layer called multiaxial perfectly matched layer (M-PML), showing no instabilities, has recently been developed.[26] This M-PML can easily be extended to the case where the CFS stretched-coordinate metrics are used in place of the ones of PML. The introduction procedure of the M-PML is in all points similar to either PML or C-PML. However, in the M-PML, the attenuation parameters σ_x and σ_y of the stretching parameters s_x and s_y are now a function of the two space variables x and y:[18,26]

$$\sigma_x(x,y) = \sigma_{xx}(x) + \sigma_{xy}(y), \tag{23a}$$

$$\sigma_y(x,y) = \sigma_{yx}(x) + \sigma_{yy}(y). \tag{23b}$$

So, all the C-PML equations given up to now, both in frequency domain [Eq. (8)] and in time domain [Eq. (16)], can be used in the M-PML with CFS stretching, just replacing, in the expressions of s_x and s_y, $\sigma_x(x)$ by $\sigma_x(x,y)$, and $\sigma_y(y)$ by $\sigma_y(x,y)$. We define as in Ref. 26 $p^x=\sigma_{yx}(x)/\sigma_{xx}(x)$ and $p^y=\sigma_{xy}(y)/\sigma_{yy}(y)$. Results obtained for medium III with $p^x=p^y=0.25$ are shown in Fig. 8. The instabilities have completely disappeared in comparison to Fig. 7, but at the expense of a stronger reflection of the waves impinging the absorbing layer with a grazing angle [Fig. 8(d)]. More details on the behavior of these stabilized absorbing layers will be given in a future publication.

In Fig. 9, snapshots of the propagation of the amplitude of the displacement in medium V are displayed for the same four different times as in medium I. Here, contrary to the case of PML,[24] no instabilities appear even at longer time. This improved stability of the C-PML over the PML has already been demonstrated theoretically by Appelö and Kreiss.[25] In fact, the "new absorbing layer" they proposed is nothing else than a new derivation of the C-PML introduced for elastic waves in Ref. 9. It can be noted that it has also been proved that the C-PML is efficient in the case of nonlinear wave absorption.[9,30]

VI. CONCLUSION

In this paper, we extend the C-PML implementation, previously made for the first-order velocity-stress formulation, to a second-order elastic wave equation written in terms of displacements both in frequency and time domains. This new formulation has been implemented in a commercial FEM software (COMSOL MULTIPHYSICS) and in a homemade PS code. The results of the simulations demonstrate that C-PMLs have more absorbing efficiency in the cases of oblique incidence and surface wave than classical PMLs.

In the case of orthotropic material stability problems have appeared, as in the first-order velocity-stress implemen-

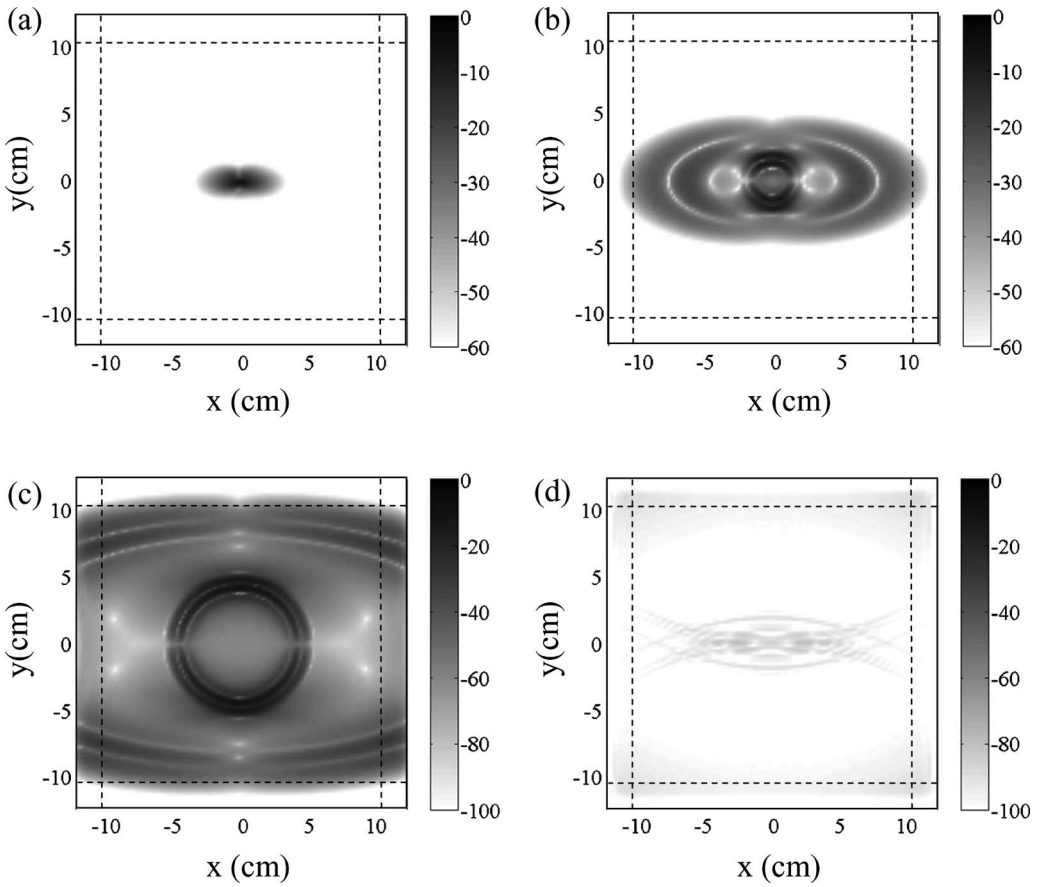

FIG. 9. Snapshots of propagation of the displacement magnitude in an orthotropic elastic medium, model V, at (a) $t=5$ μs, (b) $t=15$ μs, (c) $t=30$ μs, and (d) $t=125$ μs. The snapshots are in dB scale with a reference displacement amplitude of 10 nm.

tation. Following the "M-PML" of Meza-Fajardo and Papageorgiou,[26] we have introduced a mixture of C-PML and of sponge layer, with a controllable ratio of these two kinds of absorbing layers, in order to stabilize the C-PML, and shown that this stabilized C-PML is, in fact, not perfectly matched to the physical domain.

ACKNOWLEDGMENT

This research work was conducted, thanks to the financial support provided to the first author (Y.F.L.) in the form of a graduate scholarship by the China Scholarship Council.

[1]J. P. Bérenger, "A perfectly matched layer for the absorption of electromagnetic waves," J. Comput. Phys. **114**, 185–200 (1994).
[2]S. Gedney, "Perfectly matched layer absorbing boundary conditions," in *Computational Electrodynamics: The Finite-Difference Time-Domain Method*, edited by A. Taflove and S. C. Hagness (Artech House, Norwood, MA, 2005), Chap. 7, pp. 273–328.
[3]Q. H. Liu and J. Tao, "The perfectly matched layer for acoustic waves in absorptive media," J. Acoust. Soc. Am. **102**, 2072–2082 (1997).
[4]W. C. Chew and Q. H. Liu, "Perfectly matched layers for elastodynamics: A new absorbing boundary condition," J. Comput. Acoust. **4**, 341–359 (1996).
[5]F. D. Hastings, J. B. Schneider, and S. L. Broschat, "Application of the perfectly matched layer (PML) absorbing boundary condition to elastic wave propagation," J. Acoust. Soc. Am. **100**, 3061–3069 (1996).
[6]F. Collino and C. Tsogka, "Application of the PML absorbing layer model to the linear elastodynamic problem in anisotropic heterogeneous media," Geophysics **66**, 294–307 (2001).
[7]G. Lazzi and O. P. Gandhi, "On the optimal design of the PML absorbing boundary condition for the FDTD code," IEEE Trans. Antennas Propag. **45**, 914–917 (1997).
[8]J. A. Roden and S. D. Gedney, "Convolutional PML (CPML): An efficient FDTD implementation of the CFS-PML for arbitrary media," Microwave Opt. Technol. Lett. **27**, 334–339 (2000).
[9]O. Bou Matar, V. Preobrazhensky, and P. Pernod, "Two-dimensional axisymmetric numerical simulation of supercritical phase conjugation of ultrasound in active solid media," J. Acoust. Soc. Am. **118**, 2880–2890 (2005).
[10]F. H. Drossaert and A. Giannopoulos, "A nonsplit complex frequency-shifted PML based on recursive integration for FDTD modeling of elastic waves," Geophysics **72**, T9–T17 (2007).
[11]F. H. Drossaert and A. Giannopoulos, "Complex frequency shifted convolution PML for FDTD modeling of elastic waves," Wave Motion **44**, 593–604 (2007).
[12]D. Komatitsch and R. Martin, "An unsplit convolutional perfectly matched layer improved at grazing incidence for the seismic wave equation," Geophysics **72**, SM155–SM167 (2007).
[13]E. Bécache, P. G. Petropoulos, and S. D. Gedney, "On the long-time behavior of unsplit perfectly matched layers," IEEE Trans. Antennas Propag. **52**, 1335–1342 (2004).
[14]D. Komatitsch and J. Tromp, "A perfectly matched layer absorbing boundary condition for the second-order seismic wave equation," Geophys. J. Int. **154**, 146–153 (2003).
[15]W. C. Chew, J. M. Jin, and E. Michelssen, "Complex coordinate system as a generalized absorbing boundary condition," Microwave Opt. Technol. Lett. **15**, 363–369 (1997).
[16]M. Kuzuoglu and R. Mittra, "Frequency dependence of the constitutive parameters of causal perfectly matched anisotropic absorbers," IEEE Microw. Guid. Wave Lett. **6**, 447–449 (1996).
[17]Y. Zheng and X. Huang, "Anisotropic perfectly matched layers for elastic waves in Cartesian and curvilinear coordinates," in Earth Resources Laboratory 2002 Industry Consortium Meeting, Department of Earth Atmospheric and Planetary Sciences, Massachusetts Institute of Technology, Cambridge, MA (2002).
[18]O. Bou Matar, E. Galopin, Y. F. Li, and O. Ducloux, "An optimized

convolution-perfectly matched layer (C-PML) absorbing boundary condition for the second-order elastic wave equation—Application to surface and Lamb waves propagation," in Proceedings of the 1st European COMSOL Conference, Grenoble, France (2007).
[19]S. Ballandras, D. Gachon, J. Masson, and W. Daniau, "Development of absorbing conditions for the analysis of finite dimension elastic waveguides," in Proceedings of the IEEE International Frequency Control Symposium (2007), pp. 729–732.
[20]M. Mayer, S. Zaglmayr, K. Wagner, and J. Schöberl, "Perfectly matched layer finite element simulation of parasitic acoustic wave radiation in microacoustic devices," in Proceedings of the 2007 IEEE Ultrasonics Symposium (2007), pp. 702–706.
[21]J. P. Wrenger, "Numerical reflection from FDTD-PMLs: A comparison of the split PML with the unsplit and CFS PMLs," IEEE Trans. Antennas Propag. **50**, 258–265 (2002).
[22]M. Castaings, C. Bacon, B. Hosten, and M. V. Predoi, "Finite element predictions for the dynamic response of thermo-viscoelastic material structures," J. Acoust. Soc. Am. **115**, 1125–1133 (2004).
[23]P. Berg, F. If, P. Nielsen, and O. Skovgaard, "Analytical reference solutions," in *Modeling the Earth for Oil Exploration*, edited by K. Helbig (Pergamon, Brussels, Belgium, 1994), pp. 421–427.
[24]E. Bécache, S. Fauqueux, and P. Joly, "Stability of perfectly matched layers, group velocities and anisotropic waves," J. Comput. Phys. **188**, 399–433 (2003).
[25]D. Appelö and G. Kreiss, "A new absorbing layer for elastic waves," J. Comput. Phys. **215**, 642–660 (2006).
[26]K. C. Meza-Fajardo and A. S. Papageorgiou, "A nonconvolutional, split-field, perfectly matched layer for wave propagation in isotropic and anisotropic elastic media: Stability analysis," Bull. Seismol. Soc. Am. **98**, 1811–1836 (2008).
[27]E. Bécache and A. S. Bonnet-Ben Dhia, "PMLs for the numerical simulation of harmonic diffracted waves in an elastic plate," in Proceedings of the WCU 2003, Paris, France (2003), pp. 1019–1022.
[28]Y. F. Li, O. Bou Matar, V. Preobrazhensky, and P. Pernod, "Convolution-perfectly matched layer (C-PML) absorbing boundary condition for wave propagation in piezoelectric solid," in Proceedings of 2008 IEEE Ultrasonic Symposium (2008), pp. 1568–1571.
[29]E. A. Skelton, S. D. M. Adams, and R. V. Craster, "Guided elastic waves and perfectly matched layers," Wave Motion **44**, 573–592 (2007).
[30]D. Appelö and G. Kreiss, "Application of the perfectly matched layer to the nonlinear wave equation," Wave Motion **44**, 531–548 (2007).